Leptin regulation of *Hsp60* impacts hypothalamic insulin signaling

André Kleinridders,[1] Hans P.M.M. Lauritzen,[1] Siegfried Ussar,[1] Jane H. Christensen,[2] Marcelo A. Mori,[1] Peter Bross,[3] and C. Ronald Kahn[1]

[1]Department of Integrative Physiology and Metabolism, Joslin Diabetes Center, Harvard Medical School, Boston, Massachusetts, USA. [2]Department of Biomedicine, Aarhus University, Aarhus C, Denmark. [3]Research Unit for Molecular Medicine, Aarhus University Hospital and Aarhus University, Aarhus, Denmark.

Type 2 diabetes is characterized by insulin resistance and mitochondrial dysfunction in classical target tissues such as muscle, fat, and liver. Using a murine model of type 2 diabetes, we show that there is hypothalamic insulin resistance and mitochondrial dysfunction due to downregulation of the mitochondrial chaperone HSP60. HSP60 reduction in obese, diabetic mice was due to a lack of proper leptin signaling and was restored by leptin treatment. Knockdown of *Hsp60* in a mouse hypothalamic cell line mimicked the mitochondrial dysfunction observed in diabetic mice and resulted in increased ROS production and insulin resistance, a phenotype that was reversed with antioxidant treatment. Mice with a heterozygous deletion of *Hsp60* exhibited mitochondrial dysfunction and hypothalamic insulin resistance. Targeted acute downregulation of *Hsp60* in the hypothalamus also induced insulin resistance, indicating that mitochondrial dysfunction can cause insulin resistance in the hypothalamus. Importantly, type 2 diabetic patients exhibited decreased expression of *HSP60* in the brain, indicating that this mechanism is relevant to human disease. These data indicate that leptin plays an important role in mitochondrial function and insulin sensitivity in the hypothalamus by regulating HSP60. Moreover, leptin/insulin crosstalk in the hypothalamus impacts energy homeostasis in obesity and insulin-resistant states.

Introduction

A central feature of type 2 diabetes is insulin resistance, a state in which tissues in the body exhibit abnormal responses to normal levels of insulin. In peripheral tissues, such as liver, adipose tissue, and skeletal muscle, this is often associated with mitochondrial dysfunction (1). This dysfunction can lead to the generation of ROS, resulting in even greater levels of insulin resistance (2). The CNS is especially vulnerable to oxidative stress, since the brain consumes large amounts of oxygen (3, 4). Recently, it has been shown that oxidative stress can cause CNS damage in type 1 diabetic rodents, especially in cortical and hippocampal regions (5, 6). In addition, mitochondria from brain of type 2 diabetic rats are highly susceptible to oxidative stress and exhibit decreased antioxidant enzymes (7). Likewise, mice fed a high-fat diet have been shown to exhibit mitochondrial dysfunction in the hypothalamus and hippocampus (8, 9).

A crucial protein required for the maintenance of mitochondrial integrity and cell viability is the molecular chaperone heat shock protein 60 (HSP60) (10, 11). HSP60 forms heptameric ring complexes that, together with the HSP10 co-chaperone, enable proper folding of mitochondrial proteins in response to oxidative stress (12–15). HSP60 is crucial for cell survival, and whole-body *Hsp60* deficiency leads to cellular apoptosis and early embryonic death in mice (12, 16, 17). Missense mutations in the gene encoding HSP60 in humans (*HSPD1*) are associated with two neurodegenerative diseases: hereditary spastic paraplegia SPG13 and a fatal demyelinating leukodystrophy, indicating that neurons are especially vulnerable to the malfunction of HSP60 (18, 19).

HSP60 may also play a role in the regulation of mitochondrial function in type 2 diabetes and obesity. It has been shown that leptin is able to modulate the expression of HSP60 in pancreatic acinar cells in culture (20), and leptin has been shown to decrease oxidative stress in the CNS. Indeed, hippocampal neurons of leptin receptor–deficient (db/db) mice are prone to seizure-induced hippocampal damage, and i.c.v. leptin treatment of C57Bl/6 mice protects neurons against seizures. This effect is dependent on the activation of the JAK/STAT3 pathway and mitochondrial stabilization (21). Besides leptin's neuroprotective effect via mitochondrial stabilization, it has been shown that leptin modulates insulin signaling. Thus, hypothalamic injection of leptin leads to the phosphorylation and activation of AKT, thereby increasing insulin sensitivity in the hypothalamus and demonstrating the interplay between these pathways (22, 23). Conversely, impairment in JAK/STAT3 signaling, a key feature of leptin resistance, is often accompanied by insulin resistance (23, 24).

In the present study, we investigated whether HSP60 might play a role in hypothalamic insulin resistance and mitochondrial dysfunction in type 2 diabetes. We show that diabetic mice and humans exhibit reduced HSP60 in the brain and reduced hypothalamic insulin signaling in mice and that this is associated with mitochondrial dysfunction and reduced *Hsp60* expression. We demonstrate that leptin regulates the expression of *Hsp60* in vitro and in vivo in the hypothalamus in a JAK/STAT3-dependent manner and that knockdown of *Hsp60* in hypothalamic cells leads to mitochondrial dysfunction and insulin resistance due to increased oxidative stress. Likewise, we show that heterozygous deletion of *Hsp60* in vivo leads to mitochondrial dysfunction and insulin resistance in the hypothalamus. Strikingly, we found that acute downregulation of *Hsp60* in the hypothalamus by bilateral lentiviral injection of shRNA against *Hsp60* into the ventral hypothalamus induced insulin resistance, indicating that mitochondrial dysfunction can be a causal factor for insulin resistance in the brain. Thus,

HSP60 and its regulation by leptin are crucial for normal mitochondrial function in the hypothalamus, and HSP60 is a novel integrator that regulates insulin and leptin crosstalk in the brain.

Results

db/db mice suffer from hypothalamic insulin resistance and mitochondrial dysfunction. To assess hypothalamic insulin signaling, 12-week-old control and db/db mice were given 5 U insulin by injection into the vena cava, were sacrificed after 10 minutes, and the arcuate nucleus was isolated. The extracted proteins were subjected to SDS-PAGE and Western blotting. In control mice, there was a 2-fold increase in phosphorylation of AKT and a 1.4-fold increase in ERK activation following peripheral insulin injection, and this was reduced by approximately 50% in db/db mice (Figure 1A and Supplemental Figure 1A; supplemental material available online with this article; doi:10.1172/JCI67615DS1). This correlated with increased Ser307 phosphorylation of IRS1 in hypothalamic samples of db/db mice compared with controls (Figure 1, B and C). Increased serine phosphorylation of IRS1 can be induced by stress kinase activity following cytokine stimulation or oxidative stress due to mitochondrial dysfunction. Consistent with this, db/db mice exhibited a 2.5-fold increase in JNK phosphorylation, indicating activation of the stress kinase JNK (Figure 1, B and C).

To assess hypothalamic function, isolated mitochondria were prepared from hypothalamic samples of db/+ and db/db mice, and mitochondrial function was assessed using the Seahorse XF24 Extracellular Flux Analyzer. This revealed a 58% ± 9% decrease in the basal oxygen consumption rate (OCR) of hypothalamic mitochondria in db/db mice (Figure 1D). Maximal respiratory capacity, assessed after the addition of the uncoupling agent carbonyl cyanide-p-trifluoromethoxyphenylhydrazone (FCCP), was also reduced by 52% ± 4% in db/db mice, indicative of impaired mitochondrial respiration (Figure 1E).

The mitochondrial chaperone HSP60 is essential for normal mitochondrial integrity and function. Quantitative PCR (qPCR) analysis of db/db hypothalamic samples showed a 43% ± 8% reduction of *Hsp60* mRNA. This was paralleled by a 64% ± 4% decrease in HSP60 at the protein level as determined by Western blot analysis, with no change in the mitochondrial protein voltage-dependent anion channel (VDAC) (Figure 1, F–H). To analyze whether HSP60 was specifically downregulated in the mitochondria and also in other cellular compartments, we separated mitochondria and plasma membrane from cytoplasm using differential centrifugation in isotonic sucrose medium (25). This revealed a 49% ± 6% and 43% ± 6% reduction of HSP60 in mitochondria and cytoplasm, respectively (Supplemental Figure 1, B and C). Similar results were obtained using hypothalamus from ob/ob mice, which lack leptin, with a 24% ± 8% reduction in *Hsp60* mRNA and a 59% ± 5% reduction in HSP60 protein levels compared with control (Figure 1, I–K). Furthermore, mice fed a high-fat diet for 14 weeks revealed a 6-fold increase in serum leptin levels, a sign of leptin resistance (Supplemental Figure 1D). These mice displayed a 59% ± 10% reduction in HSP60 protein levels in the hypothalamus compared with mice fed a normal chow diet (Figure 1L). High-fat diet–fed mice also exhibited a 2.5-fold increase in IRS1 Ser307 phosphorylation in the hypothalamus, showing that diet-induced obesity causes central insulin resistance and is also associated with decreased HSP60 levels (Figure 1M). More importantly, human brain samples from controls and patients with type 2 diabetes mellitus also exhibited a 49% ± 4% reduction in *HSP60* mRNA, as assessed by qPCR analysis (Figure 1N), showing that this mechanism can be important in humans with diabetes as well. Samples from diabetic patients also revealed a 45% ± 6% reduction in STAT5B expression levels, indicative of signs of leptin resistance in these patients (Supplemental Figure 1E).

Impaired mitochondrial respiration in the hypothalamus is HSP60 dependent and induces oxidative stress. To determine whether a reduction in HSP60 could lead to the observed mitochondrial dysfunction in db/db mice, we stably transfected murine hypothalamic N25/2 cells with lentivirus containing shRNA directed against *Hsp60*. Western blot analysis of HSP60 knockdown (HSP60 KD) cells demonstrated an 80% reduction in HSP60 protein levels compared with cells infected with a scrambled control shRNA (Figure 2A). We conducted Seahorse analysis of HSP60 KD cells, which revealed 50%–60% reductions in basal respiration and maximal respiratory capacity, mimicking the changes observed in isolated mitochondria from db/db mice (Figure 2, B and C). Our assessment of mitochondrial volume using MitoTracker green revealed a significant 1.6-fold increase in HSP60 KD cells compared with control cells (Figure 2D). It is known that mitochondrial stress can lead to enlarged and swollen mitochondria (26, 27). We performed electron microscopy of HSP60 KD cells, which revealed enlarged mitochondria with a ruptured mitochondrial matrix structure (Figure 2E and Supplemental Figure 2), indicating a crucial role of HSP60 in maintaining mitochondrial integrity. This increase in mitochondrial volume and morphological abnormality was associated with a decrease in mitochondrial DNA, as qPCR revealed a 30%–40% reduction in the mitochondrial DNA content of several mitochondrial-encoded genes, including *ND1*, *rRNA*, *COX2*, and *COX3*, compared with a representative nuclear gene (Figure 2F), further supporting the observation that increased mitochondrial volume in HSP60 KD cells was due to enlarged mitochondria rather than an increase in mitochondrial numbers. Western blot analysis of protein extracts from HSP60 KD cells revealed reduced levels of complex I subunit NDUFA9, complex II subunit SDHB, complex III subunit UQCRC1, complex V subunit α subunit ATP5a1, and cytochrome B (Figure 2G). This occurred with no change in mRNA expression for these proteins (Figure 2H), consistent with a change in protein turnover secondary to a defect in protein folding in the absence of HSP60. Likewise, citrate synthase, an enzyme whose folding is known to be facilitated by HSP60 (28), exhibited a 22% ± 4% ($P \leq 0.05$) (Supplemental Figure 2) decrease in protein levels and a 17% ± 7% ($P = 0.052$) decrease in activity (Figure 2I).

Mitochondrial stress not only results in swollen and ruptured mitochondria, but often results in an increased production of ROS. Staining with the fluorescent dye MitoSOX red revealed a 2-fold increase in ROS in HSP60 KD cells compared with control (Figure 2J). This was associated with a 1.5-fold increase in lipid peroxidation determined as thiobarbituric acid reactive substances (TBARS) (Figure 2K). Thus, an absence of HSP60 leads to enlarged and ruptured mitochondria and increased oxidative stress.

HSP60 is a leptin-induced mitochondrial chaperone. Leptin resistance is a common feature of human obesity and is associated with insulin resistance and mitochondrial dysfunction (29). Conversely, leptin treatment has been shown to regulate mitochondrial function (21). To determine the possible role of leptin in the regulation of HSP60 at the level of the hypothalamus, leptin (2 μg/g BW) was twice daily injected into 12-week-old leptin-deficient ob/ob mice. This resulted in a 3-fold ($P \leq 0.05$) increase in HSP60 protein levels from the arcuate nucleus (Figure 3A). Likewise, injecting leptin into C57Bl/6 mice
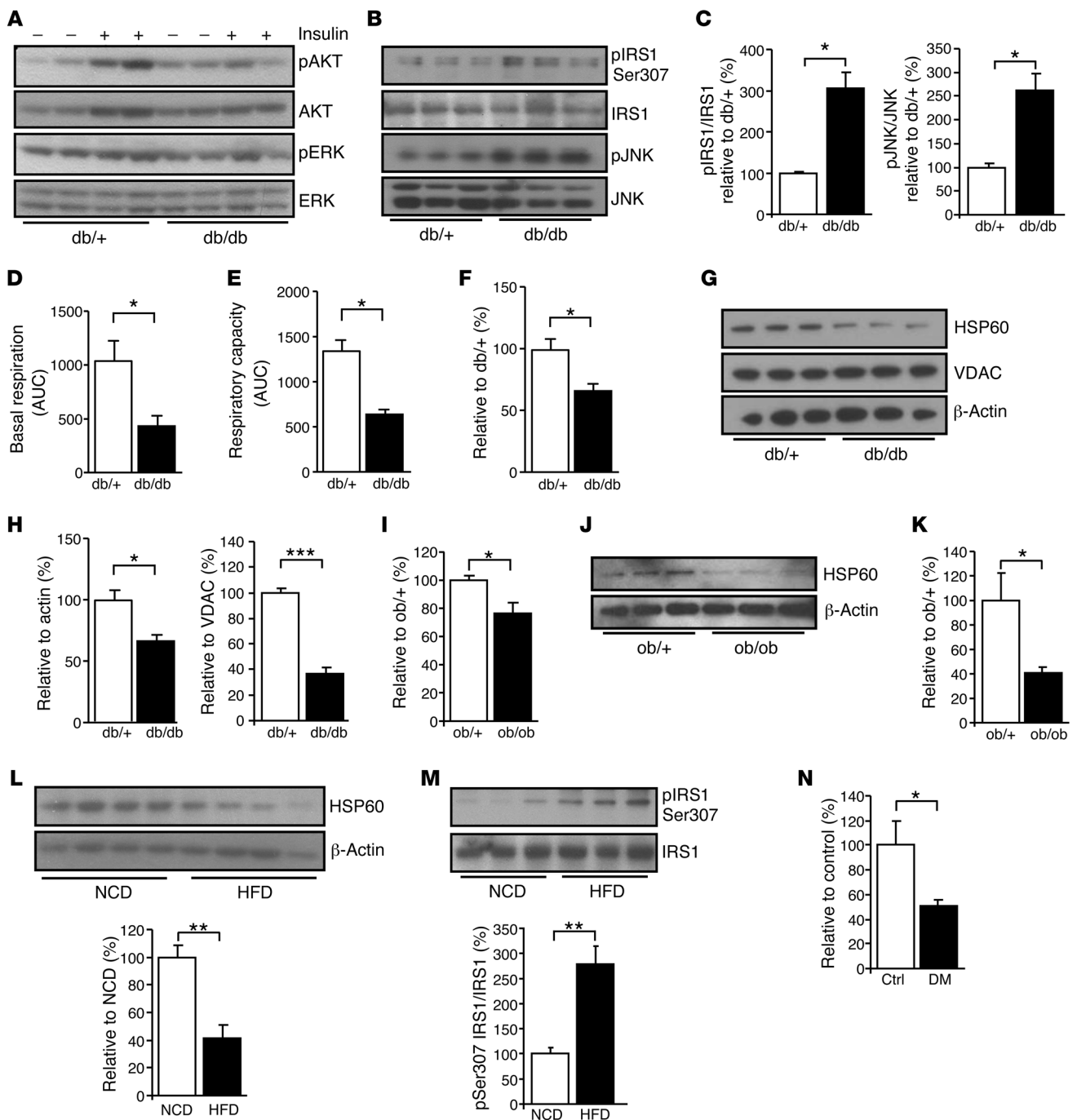
Figure 1

HSP60 reduction is associated with central insulin resistance. (**A**) Western blot analysis of phosphorylated AKT and ERK of dissected arcuate nuclei of control and db/db mice. Experiment was repeated twice with a total of six for each genotype. See Supplemental Figure 1 for densitometric analysis. (**B**) Western blot and (**C**) densitometric analysis of phosphorylated IRS1 Ser307 and JNK in hypothalami of db/+ and db/db mice ($n = 3$ for each). (**D**) Basal respiration and (**E**) respiratory capacity measurements, displayed as AUC, of isolated mitochondria dissected from hypothalami of db/+ and db/db mice ($n = 3$ for each). (**F**) Gene expression ($n = 6$ each) and (**G**) Western blot analysis of HSP60 in dissected hypothalami from db/+ mice and db/db mice ($n = 3$ each). (**H**) Densitometric analysis of HSP60 relative to β-actin and VDAC from db/+ and db/db mice ($n = 3$ each). (**I**) Gene expression ($n = 6$ each) and (**J**) Western blot analysis of HSP60 in dissected hypothalami of ob/+ mice and ob/ob mice ($n = 3$ each). (**K**) Densitometric analysis of HSP60 relative to β-actin of ob/+ and ob/ob mice. (**L**) Western blot and densitometric analysis of HSP60 and (**M**) phosphorylated IRS1 Ser307 in hypothalami of mice fed a normal chow diet (NCD) or a high-fat diet (HFD) ($n = 4–5$ each). (**N**) Gene expression analysis of *HSP60* in dissected human brain samples of controls ($n = 3$) and patients with diabetes mellitus (DM) ($n = 4$). Displayed values are the means ± SEM. *$P \leq 0.05$; **$P \leq 0.01$; ***$P \leq 0.001$.
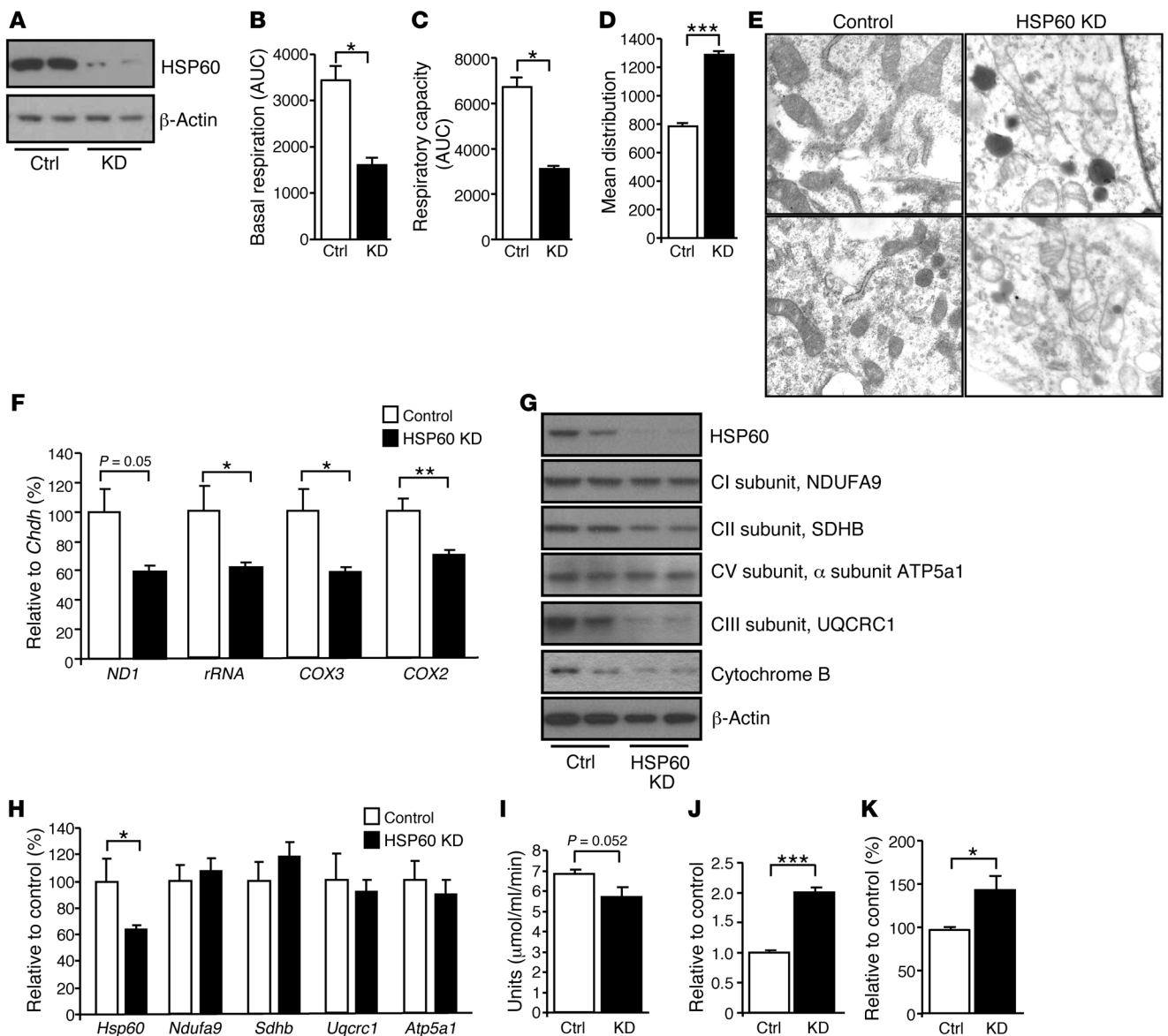
Figure 2

Impaired mitochondrial respiration in the hypothalamus is HSP60 dependent and induces oxidative stress. (**A**) Western blot analysis of HSP60 in N25/2 cells infected with a lentiviral *Hsp60* shRNA or scrambled shRNA. (**B**) Basal respiration and (**C**) maximal respiratory capacity measurements, displayed as area under the curve, of control and HSP60 KD cells. (**D**) Assessment of mitochondrial volume using MitoTracker green staining in control and HSP60 KD cells (*n* = 3 each). (**E**) Electron microscopy from mitochondria of control and HSP60 KD cells. Scope magnification, ×19,000; enlargement magnification, ×2.45; total magnification, ×46,550. (**F**) Mitochondrial DNA compared with genomic DNA content (*n* = 6 each). (**G**) Western blot analysis of nuclear- and mitochondrial-encoded genes in control (*n* = 2) and HSP60 KD cells *n* = 2 each). The experiment was performed twice with a total of four per group. (**H**) Gene expression analysis of analyzed nuclear- and mitochondrial-encoded proteins. (**I**) Citrate synthase activity in control and HSP60 KD cells (*n* = 8 each). (**J**) Quantification of superoxide accumulation using MitoSOX staining of control and HSP60 KD cells (*n* = 3 each). (**K**) Quantification of lipid peroxidation using TBARS assay on control (*n* = 5) and HSP60 KD cells (*n* = 6). Displayed values are the means ± SEM. *$P \leq 0.05$; **$P \leq 0.01$; ***$P \leq 0.001$.

fasted for 18 hours led to a 2-fold increase in HSP60 protein levels in the arcuate nucleus (Supplemental Figure 3). Additionally, refeeding fasted C57Bl/6 mice produced a 3.6-fold increase in serum leptin levels, and this was accompanied by a 36% ± 5% increase in hypothalamic HSP60 levels (Figure 3, B and C). To determine whether leptin directly regulates HSP60 expression, SK-N-SH human neuroblastoma cells were treated in vitro with 10 nM leptin, and *Hsp60* mRNA

and protein expression was determined. After 1 hour of leptin treatment, there was a modest 28% ± 4% (*P* = 0.042) increase in *Hsp60* mRNA (Figure 3D), but a greater than 2-fold increase in HSP60 protein (Figure 3E). To determine whether this was due to a direct transcriptional effect, SK-N-SH cells were transiently transfected with a luciferase reporter construct under the control of the human *HSP60* promoter, serum starved, and treated with either 10% FBS
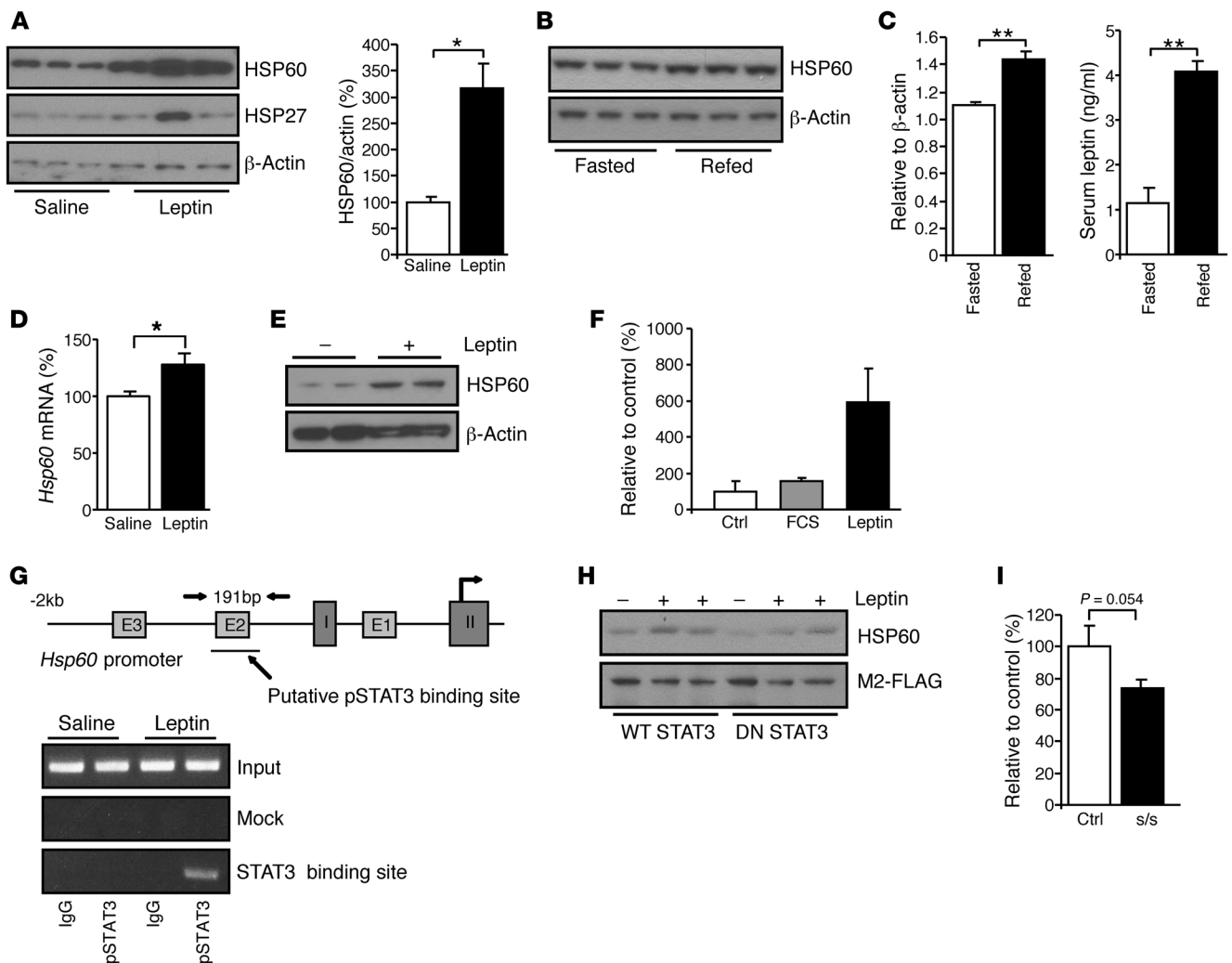
Figure 3
HSP60 is a leptin-induced mitochondrial chaperone. (**A**) Western blot and densitometric analysis of HSP60 in arcuate nuclei of ob/ob mice after saline or leptin treatment. (**B**) Western blot and (**C**) densitometric analysis of HSP60 in arcuate nuclei of fasted or refed C57BL/6 mice and serum leptin levels ($n = 3$ for each group). (**D**) Gene expression ($n = 4$ each) and (**E**) Western blot analysis of HSP60 in SK-N-SH cells after treatment with saline or leptin. This experiment was repeated twice with a total of four for each genotype. (**F**) Luciferase activity measurement under the control of the human *HSP60* promoter after leptin stimulation ($n = 4$ for each stimulation). (**G**) ChIP analysis of pSTAT3 after leptin stimulation of the *Hsp60* promoter. (**H**) Western blot analysis of HSP60 in saline- (–) or leptin-treated (+) lysates of SK-N-SH cells transfected with either WT STAT3 or DN STAT3. (**I**) Gene expression analysis of *Hsp60* in arcuate nucleus of control (Ctrl) and lepr[S1138] mice (s/s) ($n = 6$ each). Displayed values are the means ± SEM. *$P \leq 0.05$; **$P \leq 0.01$.

or 10 nM leptin for 10 hours. While FBS led to a 1.5-fold increase in luciferase activity compared with serum-starved controls, leptin produced a 6-fold increase in luciferase activity, indicating that leptin can directly regulate HSP60 on a transcriptional level above the induction by general growth factor stimulation (Figure 3F).

Leptin is known to stimulate STAT3 phosphorylation (30), and in silico analysis of the first 2 kb of the murine *Hsp60* gene promoter revealed a putative STAT3 binding site near the E2 box at positions –80 to –88 in the *Hsp60* promoter (31). To determine whether this might be involved in leptin regulation of *Hsp60* transcription, we performed ChIP experiments using anti–P-STAT3 antibody on SK-N-SH cell lysates untreated or stimulated with 10 nM leptin for 1 hour. Whereas lysates from untreated cells or cells treated with leptin and immunoprecipitated with control anti-IgG showed no

interaction, following leptin stimulation, we detected increased STAT3 binding to the *Hsp60* promoter immunoprecipitated with anti–P-STAT3, indicating that leptin induces HSP60 via the induction and binding of STAT3 to its binding site in the *Hsp60* promoter (Figure 3G). Consistent with this, SK-N-SH cells transfected with wild-type STAT3 (WT STAT3) cDNA and stimulated with 10 nM leptin for 1 hour exhibited an upregulation of HSP60 by Western blotting, whereas leptin had no effect in samples transfected with dominant-negative STAT3 (DN STAT3), showing that functional STAT3 signaling is necessary in leptin's action to induce HSP60 levels (Figure 3H). To further confirm that HSP60 is regulated in a leptin-STAT3–dependent manner in vivo, we assessed *Hsp60* gene expression in knockin mice expressing a leptin receptor with a mutation at the STAT3 activation site (lepr[S1138]) (32). This mouse
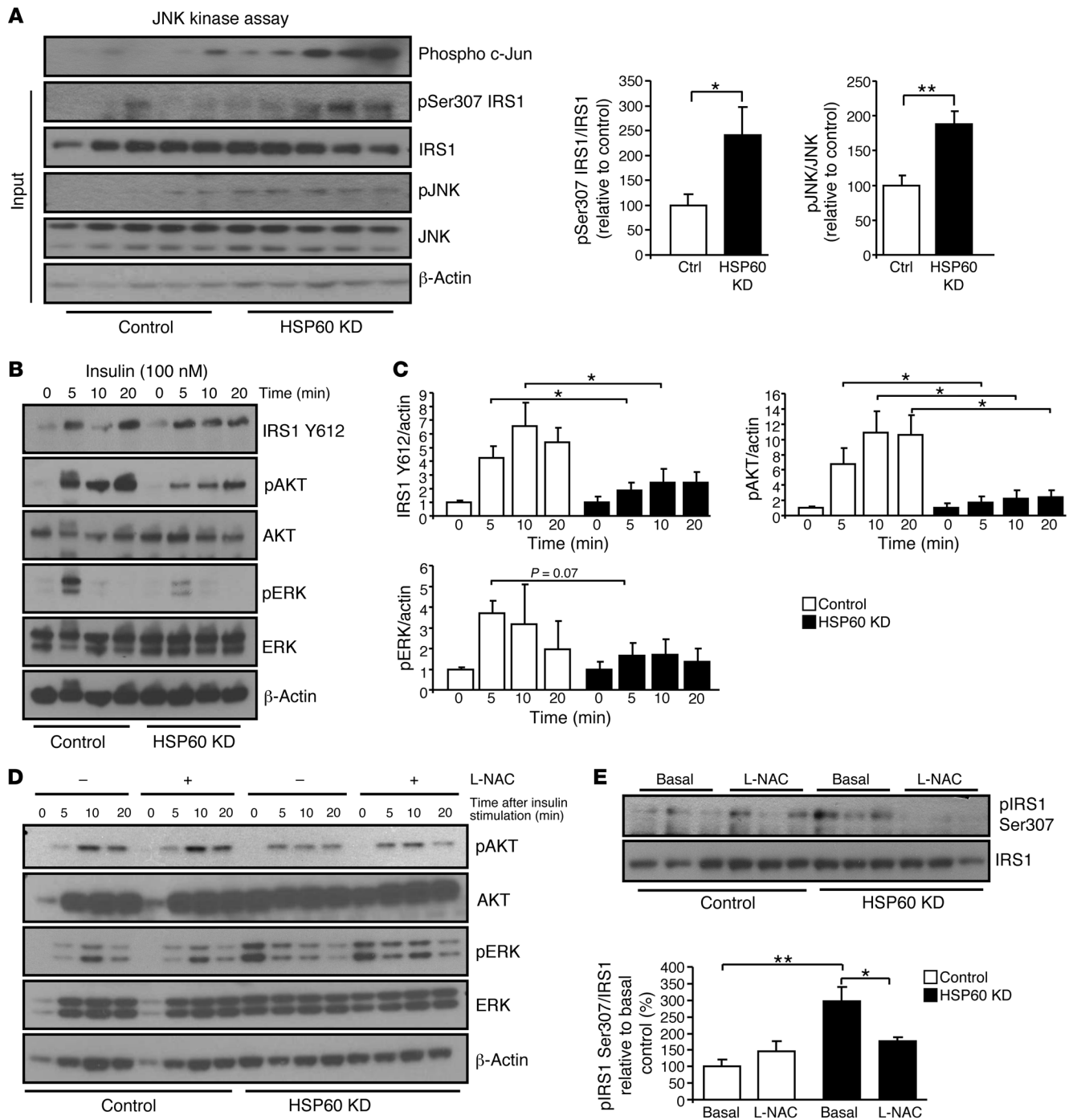
Figure 4
Downregulation of HSP60 causes insulin resistance and can be reversed upon antioxidant treatment. (**A**) JNK kinase assay as measured by c-Jun phosphorylation and Western blot analysis of phosphorylated IRS1 Ser307 and phosphorylated JNK in control and HSP60 KD cells ($n = 5$ each). The experiment was performed three times with a total of 10 per group. (**B**) Western blot and (**C**) densitometric analysis of insulin-stimulated phosphorylation of IRS1, AKT, and ERK in control and HSP60 KD cells ($n = 7$). (**D**) Western blot analysis of insulin-stimulated phosphorylation of AKT and ERK in control and HSP60 KD cells pretreated with saline or 3.5 mM L-NAC. (**E**) Western blot and densitometric analysis of phosphorylated IRS1 Ser307 in control and HSP60 KD cells treated with L-NAC. Displayed values are the means ± SEM. *$P \le 0.05$; **$P \le 0.01$.

exhibited an approximately 30% decrease in *Hsp60* in the arcuate nucleus (Figure 3I), further confirming that *Hsp60* can also be regulated via leptin-dependent STAT3 activation in vivo. Together, these data demonstrate that leptin, acting via STAT3 signaling, is a

regulator of HSP60 expression in neuronal cells, allowing leptin to regulate HSP60 in different nutritional states.

Downregulation of HSP60 in hypothalamic cells causes insulin resistance and can be reversed upon antioxidant treatment. Altered mitochondrial

function and accumulation of ROS can lead to activation of the stress kinases, which can serine phosphorylate IRS1 proteins, resulting in a decrease in tyrosine phosphorylation of IRS1 and insulin resistance (33). Western blot analysis of cells in which HSP60 had been knocked down demonstrated a 2-fold increase in phosphorylation and activation of the stress kinase JNK and a 2-fold increase in IRS1 Ser307 phosphorylation in the basal state compared with controls (Figure 4, A and B). Following stimulation with 100 nM insulin, the control cells exhibited an increase in tyrosine phosphorylation of IRS1 and phosphorylation and activation of AKT and ERK, peaking at 5 minutes; all these responses showed an approximately 50%–80% reduction in HSP60 KD cells (Figure 4C). Stimulation of HSP60 KD cells with 10 nM IGF1 also revealed decreased IRS1 tyrosine phosphorylation, as well as decreased phosphorylation of its downstream signals including AKT and ERK (Supplemental Figure 4A).

To address whether increased oxidative stress was responsible for the observed insulin resistance phenotype, we treated control and HSP60 KD cells with the antioxidant N-acetyl-L-cysteine (L-NAC) for 24 hours, followed by stimulation with 100 nM insulin for 5 to 20 minutes. Pretreatment with L-NAC reversed the insulin resistance phenotype by increasing phosphorylation of AKT and ERK in HSP60 KD cells, while having no effect on the control cells (Figure 4D). In addition, phosphorylation of IRS1 Ser307 was decreased by 41% ± 4% in HSP60 KD cells pretreated with L-NAC and was indistinguishable from the control cells, indicating that reducing oxidative stress rescues the insulin resistance phenotype in HSP60 KD cells (Figure 4E). Treatment of cells with a different antioxidant, ascorbic acid, confirmed the observed phenotype and demonstrated that pretreatment with an antioxidant can reverse the insulin-resistant phenotype in HSP60 KD cells (Supplemental Figure 4B). Thus, reduced expression of HSP60 leads to increased mitochondrial stress and oxidative stress, increased IRS1 Ser307 phosphorylation, and resistance to insulin and IGF1 signaling, and this can be blocked by antioxidant treatment.

Hsp60$^{+/-}$ mice display insulin resistance in the arcuate nucleus. To confirm these results in vivo, we used mice with heterozygous KO of *Hsp60* (*Hsp60$^{+/-}$*). These mice are viable, in contrast to homozygous KO mice and exhibit a 40%–50% reduction of HSP60 in the hypothalamus and other tissues, comparable to the reduced levels of HSP60 observed in db/db mice (Figure 5A). HSP60 heterozygous KO mice displayed unaltered body weight and composition, unaltered food intake, and normal orexigenic and anorexigenic neuropeptide expression in the hypothalamus and were normoglycemic compared with controls (Supplemental Figure 5). *Hsp60$^{+/-}$* female mice were insulin resistant, and males showed a trend toward insulin resistance (Supplemental Figure 5).

Using mitochondria isolated from hypothalamus, we performed Seahorse analysis, which revealed an approximately 30% reduction in basal respiration in *Hsp60$^{+/-}$* mice compared with control (*P* = 0.035), and maximal respiratory capacity was reduced by approximately 22%, although the latter did not quite reach significance (Figure 5, B and C). We found that this alteration in mitochondrial activity was also evident in vivo, using 2-photon microscopy to assess NADH content in freshly isolated hypothalamic brain slices of control and *Hsp60$^{+/-}$* mice. This analysis revealed a 75% ± 6% decrease in NADH content in *Hsp60$^{+/-}$* mitochondria compared with control in the arcuate nucleus, reflecting reduced mitochondrial activity (Figure 5, D and E). MitoTracker green staining revealed a 1.5-fold increase in mitochondrial volume in hypothalamus of *Hsp60$^{+/-}$* mice compared with control (Figure 5F). Furthermore, Western blot analysis showed reduced amounts of electron transport chain proteins such as complex V α (25% ± 2%), complex III core 2 (16% ± 2%), and complex IV-I (34% ± 8%) (all *P* < 0.05) in extracts isolated from hypothalamus of *Hsp60$^{+/-}$* mice compared with control (Supplemental Figure 2). Thus, a reduction in HSP60 leads to mitochondrial dysfunction in vitro and in vivo.

This mitochondrial dysfunction led to a 1.5-fold increase in phosphorylation of JNK and a 1.8-fold increase in IRS1 Ser307 phosphorylation in *Hsp60$^{+/-}$* mice compared with control (Figure 5, G and H). Furthermore, insulin stimulation by injection into the vena cava revealed increased phosphorylation of AKT and ERK in protein lysates from isolated arcuate nuclei of control mice, whereas it was reduced in *Hsp60$^{+/-}$* mice (Figure 5I), confirming that mitochondrial dysfunction produced by reduced levels of HSP60 can lead to insulin resistance in vitro and in vivo.

Acute HSP60 reduction in the hypothalamus causes insulin resistance. To address the question of whether acute HSP60 deficiency causes insulin resistance, we bilaterally injected a lentivirus containing shRNA directed against *Hsp60* (HSP60 KD) or a scrambled control into the ventral hypothalamus. This resulted in a 25% reduction in *Hsp60* mRNA and an approximately 40% reduction in HSP60 protein in the hypothalamus (Figure 6, A and B). One week after injection, HSP60 KD mice were normoglycemic, had unaltered food intake, and showed no difference in the expression of orexigenic and anorexigenic neuropeptides in the hypothalamus (Figure 6, C–E). However, Western blot analysis revealed a 6.8-fold increase in IRS1 Ser307 phosphorylation and a 2.5-fold increase in phosphorylation of JNK in the hypothalamus of HSP60 KD animals compared with controls, indicating that acute knockdown of *Hsp60* in the hypothalamus can cause insulin resistance (Figure 6, F and G). Additionally, qPCR analysis revealed a 2-fold increase in SOCS3 levels in the hypothalamus of HSP60 KD mice. SOCS3 has been shown in other studies to induce insulin and leptin resistance (34, 35). Furthermore, downregulation of HSP60 caused a substantial proinflammatory response in the hypothalamus, with increases in inflammatory markers such as TNF-α, MCP-1, IL-6, and IL-1β, but no increases in apoptotic proteins, as assessed by gene expression and Western blot analysis (Figure 6H and Supplemental Figure 6). These data demonstrate that acute downregulation of *Hsp60* in the hypothalamus causes insulin resistance in vivo.

Discussion

Leptin and insulin act as anorectic signals in the hypothalamus to reduce food intake and increase energy expenditure (24). Leptin action in hypothalamic neurons depends on activation of the JAK/STAT3 pathway, and both leptin and insulin stimulate PI3 kinase, leading to crossactivation of these pathways (22, 36). The importance of hypothalamic insulin signaling is demonstrated by ablation of the insulin receptor in the CNS, resulting in increased food intake, obesity, and reduced fertility (37). In addition, central insulin signaling regulates hepatic glucose production, and central insulin resistance causes derepression of hepatic gluconeogenesis (38, 39). All of these features are characteristics of type 2 diabetes, suggesting that central insulin resistance may be an important component of, and a potential target for, future treatments for diabetes and metabolic syndrome.

In the present study, we show that type 2 diabetic mice and humans exhibited reduces *Hsp60* mRNA in brain and that in
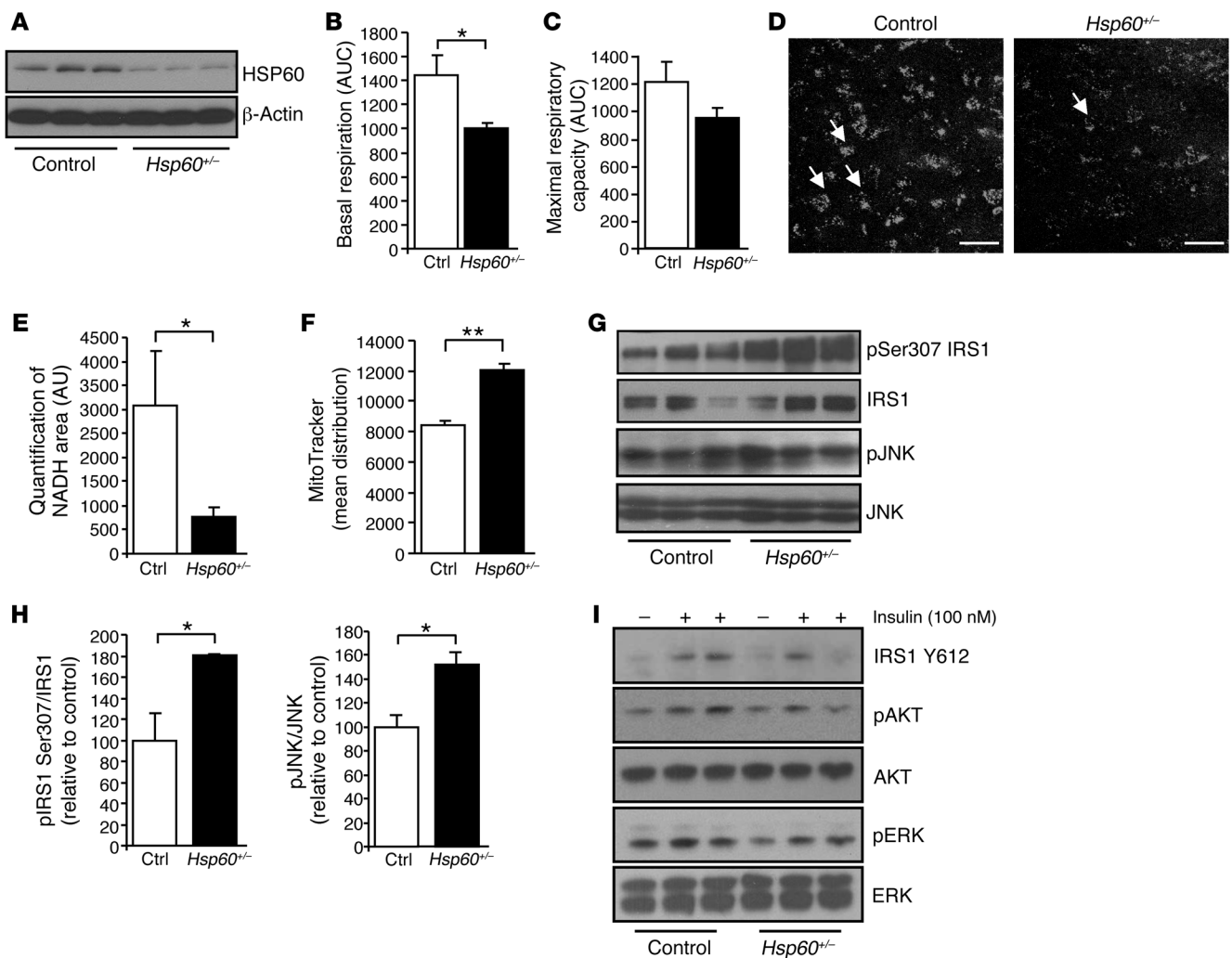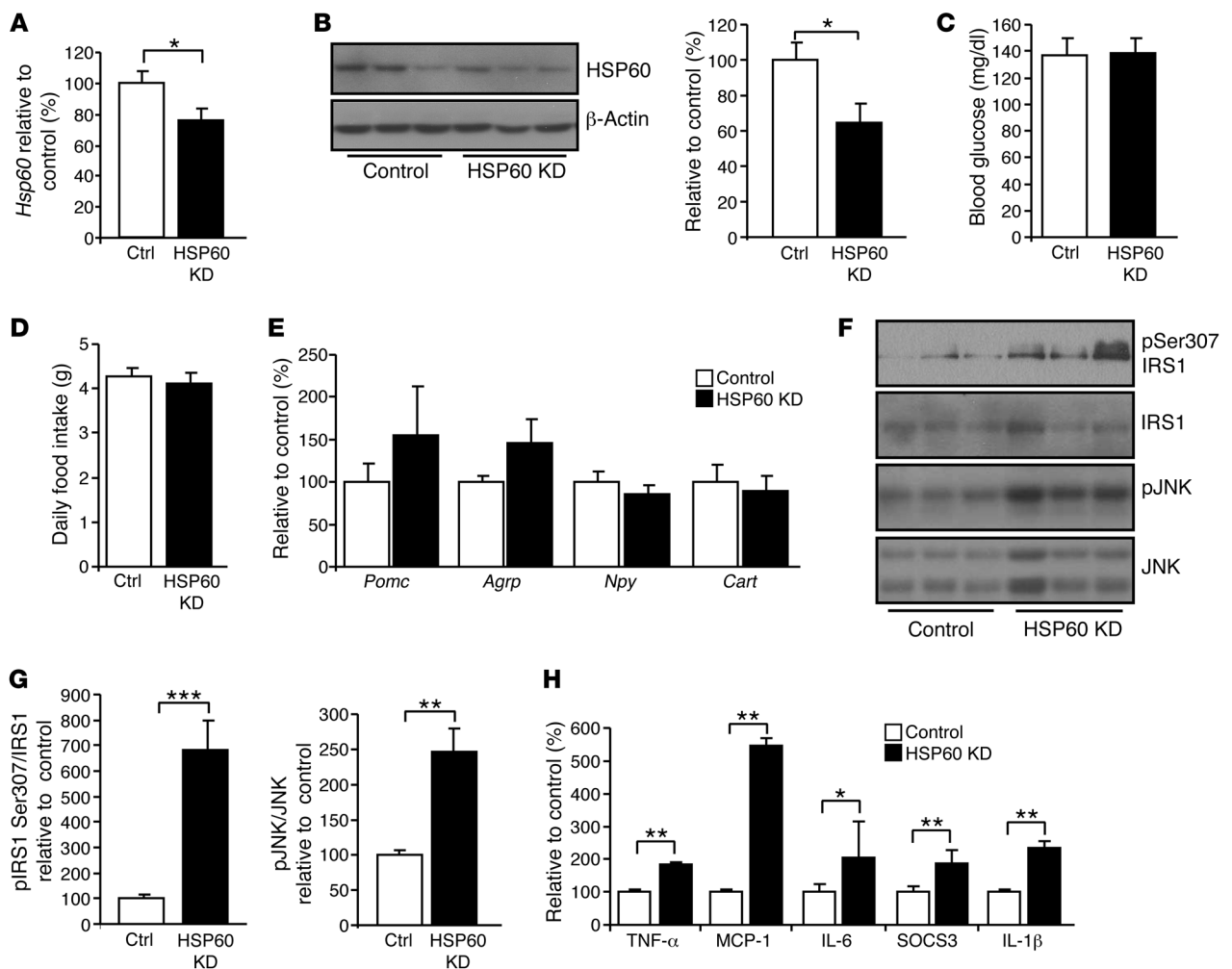
Figure 5

Hsp60⁺/⁻ mice suffer from mitochondrial dysfunction and insulin resistance in the arcuate nucleus. (**A**) Western blot analysis of HSP60 in arcuate nuclei of control and *Hsp60⁺/⁻* mice. (**B**) Basal respiration and (**C**) maximal respiratory capacity measurements, displayed as AUC, of isolated mitochondria dissected from hypothalami of control or *Hsp60⁺/⁻* mice ($n = 4$ each). (**D**) Representative sum projections of brain-slice images of mitochondrial NADH in arcuate nucleus from control and *Hsp60⁺/⁻* mice. Arrows indicate NADH-positive mitochondrial structures. Scale bars: 50 μm. (**E**) Image quantifications of NADH-positive mitochondrial structures in control ($n = 4$) and *Hsp60⁺/⁻* mice ($n = 6$). (**F**) Assessment of mitochondrial volume on isolated hypothalamic mitochondria of control and *Hsp60⁺/⁻* mice using MitoTracker green staining ($n = 3$ each). (**G**) Western blot and (**H**) densitometric analysis of phosphorylated IRS1 Ser307 and phosphorylated JNK in dissected hypothalami from control and *Hsp60⁺/⁻* mice ($n = 5–6$ each). (**I**) Western blot analysis of insulin-stimulated phosphorylation of IRS1, AKT, and ERK in arcuate nuclei of control and *Hsp60⁺/⁻* mice. This experiment was repeated twice with a total of six for each genotype. Displayed values are the means ± SEM. *$P \leq 0.05$; **$P \leq 0.01$. *Hsp60* heterozygous, *Hsp60⁺/⁻*.

obese, diabetic mice, this was also associated with central insulin resistance and mitochondrial dysfunction. We demonstrate that leptin regulates mitochondrial activity and integrity in the hypothalamus by regulating *Hsp60* expression through a STAT3-dependent pathway, ensuring proper mitochondrial function. In obese, leptin-deficient ob/ob mice, this could be reversed by leptin treatment. We found that these in vivo alterations could be mimicked in vitro by lentiviral knockdown of *Hsp60* in neurons and recapitulated in vivo by heterozygous inactivation of the *Hsp60* gene or by lentiviral knockdown of *Hsp60* in the hypothalamus. The mitochondrial dysfunction produced by the reduction in HSP60 caused oxidative stress, activation of the stress kinase JNK,

IRS1 Ser307 phosphorylation, and insulin resistance in vitro and in vivo. Pretreatment with the antioxidant L-N-acetyl-cysteine reversed the observed IRS1 Ser307 phosphorylation and insulin resistance, highlighting that a reduction in oxidative stress can improve insulin sensitivity. Thus, normal expression of HSP60 in the hypothalamus ensures mitochondrial integrity, influences insulin sensitivity, and acts as an integrator in central insulin/leptin crosstalk. Importantly, the observed reduction in HSP60 levels in diabetic mice could be confirmed in human brain samples from diabetic patients, indicating that this dysregulation is also present in diabetic patients and may play a role in the pathophysiology of human diabetes mellitus.

Figure 6
Acute HSP60 deficiency in the hypothalamus causes insulin resistance. (**A**) Gene expression and (**B**) Western blot and densitometric analysis of HSP60 in hypothalami of control and HSP60 KD mice ($n = 7$–8). (**C**) Randomly fed blood glucose levels of control and HSP60 KD mice ($n = 7$–8). (**D**) Average daily food intake of control and HSP60 KD mice ($n = 7$–8). (**E**) Gene expression analysis of orexigenic and anorexigenic neuropeptides of control and HSP60 KD mice ($n = 7$–8). (**F**) Western blot and (**G**) densitometric analysis of phosphorylated IRS1 Ser307 and JNK ($n = 7$–8). (**H**) Gene expression analysis of inflammatory markers and SOCS3 in control and HSP60 KD mice ($n = 7$–8). Displayed values are the means ± SEM. *$P \leq 0.05$; **$P \leq 0.01$; ***$P \leq 0.001$.

Altered mitochondrial function in the hypothalamus can be induced by diet and improved by insulin sensitizers. For example, Thaler et al. observed disturbed mitochondrial structure in pro-opiomelanocortin (POMC) neurons of mice fed a high-fat diet (8). Furthermore, our data show that mice fed a high-fat diet have a reduction in HSP60 protein in the hypothalamus, and this is also associated with an increase in IRS1 Ser307 phosphorylation, an indicator of insulin resistance. In addition, it has been shown that mice fed a high-fat diet for 14 weeks suffer from hippocampal insulin resistance, which is associated with mitochondrial dysfunction and increased ROS production (9). Since diet-induced obesity causes leptin and insulin resistance, it raises the possibility that these hormones can directly affect mitochondrial integrity and thus decrease cellular stress. Indeed, treatment with the insulin sensitizer rosiglitazone can reverse the insulin resistance phenotype and reduce mitochondrial dysfunction and

ROS production in the hippocampus, indicating that stabilizing mitochondrial function can improve insulin sensitivity in the brain (9). As rosiglitazone increases insulin sensitivity and reduces mitochondrial stress in the brain, it is tempting to speculate that HSP60 could play a role in this scenario.

Leptin, acting via STAT3, has been shown to increase neuronal survival by stabilizing mitochondrial integrity (21). Leptin can induce the expression of genes in the electron transport chain of the hypothalamus, indicating a direct effect of leptin on mitochondrial activity (40). Our data show that HSP60 is regulated directly by leptin by inducing the interaction of phospho-STAT3 with its putative binding site in the *Hsp60* promoter.

A major question that remains unresolved is whether insulin resistance is a cause or consequence of mitochondrial dysfunction. Multiple studies have shown that mitochondrial dysfunction is associated with insulin resistance in peripheral tissues (1).

Recent studies have shown that diet-induced obesity leads to mitochondrial dysfunction in the brain and insulin resistance (8, 9), but it has not been shown that mitochondrial dysfunction in the brain causes insulin resistance. Here, we demonstrate that mitochondrial dysfunction caused by genetic manipulation of *Hsp60* induces insulin resistance in the hypothalamus, indicating that mitochondrial dysfunction alone can induce insulin resistance. Furthermore, we found that acute downregulation of *Hsp60* via bilateral injection of a lentivirus containing shRNA against HSP60 into the hypothalamus caused insulin resistance, indicating that hypothalamic mitochondrial dysfunction can cause insulin resistance. An alteration in mitochondrial dynamics, such as increased mitochondrial fission, has been shown to cause oxidative stress in skeletal muscle and neurons (41) and insulin resistance in obese and diabetic mice (42). On the other hand, in hepatocytes, insulin signaling is sufficient to induce HSP60 (43). We observed that insulin can also induce HSP60 in neurons (data not shown), suggesting that both leptin and insulin resistance can lead to a vicious cycle of reduced HSP60, mitochondrial dysfunction, and increased insulin resistance in the hypothalamus. Not all mitochondrial dysfunction, however, is associated with insulin resistance, as exemplified by the whole-body deficiency of PGC1 α or combined ablation of PGC1 α and β in skeletal muscle (44, 45). In the latter, it is possible that insulin resistance was not observed because insulin tolerance testing is a relatively insensitive method (46), because various forms of mitochondrial dysfunction affect the organism differently (47, 48), or because certain tissues are highly susceptible to mitochondrial stress (18, 19). The fact that the brain is very susceptible to oxidative stress (49) may explain why mitochondrial dysfunction caused by decreased HSP60 levels in neurons results in insulin resistance. Interestingly, although acute downregulation of *Hsp60* in the hypothalamus causes insulin resistance with a 2-fold increase in SOCS3 expression, these mice did not show any change in food intake or alterations in orexigenic or anorexigenic neuropeptide expression. It has been shown that a prolonged increase in SOCS3 expression in POMC and AgRP neurons causes hyperphagia (50, 51), however, our data demonstrate that a short-term increase in SOCS3 expression and insulin resistance due to HSP60 dysregulation is not sufficient to alter food intake or cause obesity.

Mice with a heterozygous loss of *Hsp60*, i.e., those with an approximately 50% decrease in HSP60 protein, serve as a model for reduced expression of HSP60 in diabetic mice. These mice exhibit altered mitochondrial morphology and mitochondrial function, as assessed by the Seahorse Flux analyzer and NADH imaging in vivo and hypothalamic insulin resistance. The latter appears to be secondary to increased ROS, as reducing oxidative stress by antioxidant treatment rescues the insulin-resistant phenotype. Studies in peripheral tissues, such as skeletal muscle, have shown that reducing ROS levels by antioxidant treatment or by overexpression of antioxidant enzymes increases insulin sensitivity (52–54). We found that treatment of HSP60 KD neurons with L-NAC ameliorated insulin resistance, extending the beneficial effect of reducing augmented ROS levels in peripheral tissues and in the CNS. It is important to keep in mind that different degrees of ROS accumulation may have different effects. In fact, insulin signaling per se generates ROS, and this appears to be important for proper insulin action (55). Thus, when humans are subjected to exercise, there is an increase in markers of oxidative stress in skeletal muscle, but increased insulin sensitivity, and supplemen-

tation with antioxidants reduces the improved insulin sensitivity after exercise (56, 57). On the other hand, uncontrolled ROS generation by mitochondrial dysfunction can clearly be detrimental to insulin sensitivity in peripheral tissues (2) and the CNS (current work). Thus, there is a fine balance between oxidative stress and insulin signaling. Although whole-body *Hsp60*$^{+/-}$ mice suffer from central insulin resistance, these mice display unaltered body weight, normal glucose tolerance, and exhibit only mild insulin resistance in females. It is difficult to speculate about the role of HSP60 in different tissues in insulin signaling, since *Hsp60*$^{+/-}$ mice suffer from a 50% reduction in HSP60 in all tissues. However, even though whole-body knockout of *Hsp60* is lethal, it is not surprising that heterozygous mice do not show a strong phenotype, as mice heterozygous for the insulin receptor also show only a very mild phenotype of systemic insulin resistance (58, 59).

HSP60 is a member of a large family of molecular chaperones that might be altered in diabetes. It has been shown that ER chaperones, such as GRP78 (BiP), are upregulated in obese states and are associated with insulin resistance (60), while type 2 diabetic patients display reduced levels of the cytosolic chaperone heat shock protein 72 (HSP72) in skeletal muscle, and this is also associated with insulin resistance (61). Our data extend the scenario of dysregulated chaperones, showing that the mitochondrial chaperone HSP60 is reduced in diabetes and influences insulin sensitivity. Weekly "heat treatment" of high-fat diet–treated mice has been shown to improve insulin resistance and hyperglycemia, suggesting that increasing heat shock response has beneficial effects on glucose and insulin sensitivity (62). In addition, heat treatment has been shown to ameliorate insulin resistance in diet-induced obesity by reducing IRS1 Ser307 phosphorylation, activating JNK, and increasing citrate synthase activity in skeletal muscle, factors being altered by HSP60 deficiency (63). Consistent with this, overexpression of cytosolic HSP72 increases insulin sensitivity in mice fed a high-fat diet by reducing the activation of stress kinases and increasing mitochondrial activity (62). Whether heat shock–induced expression of HSP60 increases insulin sensitivity remains unknown. Increased expression of HSP60 has been shown to reduce oxidative stress and increase lifespan in yeast, pointing to its vital function as a cell-protective factor (14, 64). Interestingly, long-lived mammals and birds show increased levels of HSP60 in the brain, indicating that elevated HSP60 levels are beneficial for organisms (65). In line with these data, we found that acute HSP60 downregulation induced a robust inflammatory response, indicating the importance of HSP60 for cellular homeostasis. However, this reduction in HSP60 was not sufficient to induce apoptosis, which is in contrast to the phenotype of the complete knockout of HSP60 in mice (17). It has been hypothesized that HSP60 can have proapoptotic and antiapoptotic functions. Cytosolic *Hsp60* can have a proapoptotic function by accelerating the maturation of procaspase 3 (66, 67). We found that acute downregulation of *Hsp60* in the hypothalamus did not alter caspase 3 or cleaved caspase 3 levels.

In summary, our data show that leptin plays an important role in regulating mitochondrial function in the hypothalamus by regulating the mitochondrial chaperone HSP60. This in turn influences mitochondrial function and insulin sensitivity in the hypothalamus. These data provide what we believe to be a novel pathway of leptin/insulin crosstalk in the CNS that may impact on hypothalamic control of energy homeostasis in obesity and insulin-resistant states.

Methods

Animal care. All mice were housed in a mouse facility on a 12-hour light/12-hour dark cycle in a temperature-controlled room. *Hsp60*+/− mice have previously been described (17) and were backcrossed onto a C57BL/6 background for six generations prior to the study (68). Beginning at approximately 4 weeks of age, all mice were maintained on a standard chow diet containing 22% of calories from fat, 23% from protein, and 55% from carbohydrates (Mouse Diet 9F 5020; PharmaServ). Mice were allowed ad libitum access to water and food. Eight- to 10-week-old db/db and ob/ob mice were obtained from The Jackson Laboratory and were maintained on a standard chow diet containing 22% of calories from fat, 23% from protein, and 55% from carbohydrates (Mouse Diet 9F 5020; PharmaServ). Animal care and study protocols were approved by the Animal Care Committee of Joslin Diabetes Center and were in accordance with NIH guidelines.

Human brain samples. Human tissue specimens were obtained from the Human Brain and Spinal Fluid Resource Center (VA West Los Angeles Healthcare Center, Los Angeles, California, USA), which is sponsored by NINDS/NIMH, the National Multiple Sclerosis Society, and the Department of Veterans Affairs and from an ongoing, prospective, longitudinal, population-based study of aging and cognitive decline (Adult Changes in Thought Study) (69). Brain samples were obtained from middle frontal gyrus, superior and middle temporal gyri, and frontal cortex at 9 to 23 hours postmortem.

Western blot analysis. Tissues were dissected and homogenized in radioimmunoprecipitation assay (RIPA) buffer containing 0.1% SDS with a polytron homogenizer (IKA Werke). Arcuate nuclei from 13- to 14-week-old male mice were dissected and homogenized with a mortar in 100 μl of RIPA buffer containing 0.1% SDS. Cell lysates from cell culture experiments were resuspended and homogenized in 100 μl of RIPA buffer containing 0.1% SDS. Protein (10 μg) was subjected to SDS-PAGE, transferred to PVDF membranes, and blotted with antibodies raised against HSP60 (4870), HSP27 (2442), p-Ser473-AKT (9271), IRS1 (2382), p-Ser307-IRS1 (2381), p-Thr202/204-ERK1/2 (9101), ERK (9102), AKT (9272), JNK (9252), pJNK (9251) (all from Cell Signaling); complex I (A21344), complex II (A21345), complex III (A21362), complex V (A21350), p-Y612-IRS1 (44816G) (all from Invitrogen); β-actin (sc-1616; Santa Cruz Biotechnology Inc.) and cytochrome B (sc-11436; Santa Cruz Biotechnology Inc.); MitoProfile Total OXPHOS Rodent WB Antibody Cocktail (MS604; MitoSciences). Appropriate secondary HRP-conjugated antibodies (Amersham) were used, and membranes were visualized using Immobilon Western HRP Substrate (Millipore). Western blots were quantified using ImageJ software (NIH). After background subtraction, each sample was normalized to an internal loading control. The average protein expression in the control samples was set to 1 or 100% and compared with protein expression in the experimental samples.

ChIP. ChIP was performed according to the manufacturer's guidelines (17-295; Millipore). Briefly, 10^7 cells were cultivated in DMEM with 10% FBS in the absence or presence of 10 nM leptin for 1 hour. Cells were washed in 1X PBS and incubated with 1% formaldehyde for 10 minutes. Cells were lysed and sonicated using a Branson digital sonifier with 30% impulse power for six impulses. For immunoprecipitation, precleared cell lysates were incubated with anti–P-Y705-STAT3 (9131; Cell Signaling Technology) or mouse IgG (Santa Cruz Biotechnology Inc.) as a negative control. Lysates were washed, eluted in Tris-EDTA buffer, and reverse cross-linked using 1% SDS and 0.1 M NaHCO₃. For PCR amplification of the target sequences, the following primers were used: P1: 5′-AGAAAAT-GCCGCGCTCCCTAC-3′; P2: 5′-GAAAGACTCGGAGGCGGAAGAA-3′; negative control A: 5′-CACTTGGAGGATACCAGAGCA-3′; negative control B: 5′-GCTCTCCAGGGTTACCTGAGC-3′.

Enzyme assays. The measurement of TBARS was performed according to the manufacturer's guidelines (10009055; Cayman Chemicals) using 10 μg of protein sample in triplicate. A citrate synthase activity assay was performed using an assay kit from Sigma-Aldrich (CS0720). A JNK kinase assay was performed using the KinaseSTAR JNK Activity Assay Kit from BioVision (K431-40).

Analysis of gene expression by qPCR. Total RNA from cell culture or hypothalamus of 13- to 14-week-old male mice was isolated using an RNeasy kit (QIAGEN). Total RNA (1 μg) was reverse transcribed in 20 μl using the High Capacity cDNA Reverse Transcription Kit (Applied Biosystems). Synthesized cDNA (10 ng) was amplified with specific primers (100 nM each) in a 10-μl PCR using a SYBR green PCR Master Mix (Applied Biosystems). Analysis of gene expression was performed using an ABI Prism 7900HT sequence detector (Applied Biosystems) with initial denaturation at 95°C for 10 minutes, followed by 40 PCR cycles, each cycle consisting of 95°C for 15 seconds, 60°C for 1 minute, and 72°C for 1 minute; SYBR green fluorescence emissions were monitored after each cycle. For each gene, mRNA expression was calculated relative to TATA-binding protein (TBP) expression. Amplification of specific transcripts was confirmed by the melting-curve profiles (cooling the sample to 68°C and heating slowly to 95°C with measurement of fluorescence) at the end of each PCR. qPCR was performed using whole-cell DNA to assess the genomic/mitochondrial DNA ratio.

Lentiviral infection. HSP60 was stably knocked down in N25/2 cells using shRNA delivered by lentiviral infection. Target sets consisting of five separate shRNA sequences for *Hsp60* (RHS4533-NM_002156; Open Biosystems) and shSCR (Open Biosystems) were cloned into pLKO1. Cell culture dishes (10-cm) of human embryonic kidney 293T cells were transiently transfected with 2.8 μg of lentiviral expression vector and the viral packaging vectors SV-E-MLV-env and SV-E-MLV using 60 μl Superfect Reagent (QIAGEN). Forty-eight hours after transfection, virus-containing medium was passed through a 0.45-μm-pore-size syringe filter. This supernatant, supplemented with filter-sterilized Polybrene (hexadimethrine bromide, 8 μg/ml), was applied to proliferating (60% confluent) cells. Twenty-four hours after infection, cells were incubated in selection medium containing 2.5 μg/ml puromycin (Invitrogen).

N25/2 and SK-N-SH cell culture and hormone stimulation. N25/2 neuronal cells (CLU110; Cedarlane) and SK-N-SH cell lines were cultivated in media containing DMEM (4.5 g/l glucose) supplemented with 10% FBS (Gemini). Cells were trypsinized and passaged at 80% confluency. Cells were fasted for 3 hours in medium containing DMEM. Insulin (100 nM) was added to the medium, and samples were taken after 0, 5, 10, and 20 minutes of insulin supplementation. The reaction was stopped by adding ice-cold PBS to cells, and homogenized lysates were subsequently used for Western blot analyses. For antioxidant treatment, cells were cultivated in the presence of 3.5 mM L-NAC or 200 μM ascorbic acid (vitamin C) for 24 hours prior to insulin stimulation. Cells were fasted for 1 hour in medium containing DMEM before leptin stimulation. Leptin (10 nM) was added to the medium, stopped after 60 minutes with ice-cold PBS, and lysates were processed for Western blot or gene expression analysis. These experiments were independently repeated at least three times.

Electron microscopy. Confluent cells were fixed using 2.5% glutaraldehyde in 0.1 M phosphate buffer for several hours at room temperature before being placed at 4°C for storage. Cells were washed several times in a 0.1-M phosphate buffer, fixed with 2% osmium tetroxide in 0.1 M phosphate buffer for 1 hour, washed again several times in 0.1 M phosphate buffer, and stored overnight at 4°C in 0.1 M phosphate buffer. Samples were incubated in ascending concentrations of ethanol, followed by several changes of propylene oxide, using a 1:1 mixture of propylene oxide and Araldite 502 epoxy resin for several hours and placed into a vacuum desiccator overnight. Subsequently, samples were embedded in Araldite 502 epoxy resin using BEEM capsules (Ted Pella Inc.) and placed into a 60°C curing oven for 48 hours. Cured resin blocks were trimmed and one-micron sections were cut on an LKB Nova ultramicrotome using glass knives. The resulting

sections were adhered to glass slides using heat, stained with a 1% methylene blue, and selected samples were prepared for electron microscopy. Thin sections of 60 to 80 nm were cut using an LKB Nova ultramicrotome and a Diatome diamond knife, placed on 75-mesh copper grids, stained using uranyl acetate and Reynolds lead citrate, and photographed using a Philips 301 transmission electron microscope.

Assessment of mitochondrial volume and superoxide detection. Mitochondrial volume was assessed using FACS. N25/2 cells (5×10^5) were stained with 50 nM MitoTracker green (MitoSciences) for 5 minutes and subsequently trypsinized. Cells were incubated in PBS and 2% BSA, and 25,000 cells were sorted and analyzed for median stain intensity. Isolated mitochondria from hypothalamus were stained with 50 nM MitoTracker green in PBS buffer containing 2% succinate and 0.2% BSA for 15 minutes and then sorted and analyzed for median stain intensity. Mitochondrial superoxide was detected using the MitoSOX superoxide indicator according to the manufacturer's instructions (M 36008; Invitrogen).

XF24 oxygen consumption assay and bioenergetics profile. Oxygen consumption of cell lines was analyzed using the XF24 Extracellular Flux Analyzer from Seahorse Bioscience. Four to six replicates of control and sh*Hsp60* N25/2 cells (60,000 per well) were plated on a 24-well XF24 V28 cell culture microplate (Seahorse Bioscience) one day before the analysis. One hour before the experiment, cells were washed and incubated in 700 µl of nonbuffered (without sodium carbonate) DMEM (4.5 g/l glucose), pH 7.4, at 37°C in a non-CO$_2$ incubator. Replicates of four to five per cell type were included in the experiment, and four wells evenly distributed within the plate were used for correction of temperature variations. Oxygen concentration was measured over time periods of 3 minutes at 7-minute intervals, consisting of a 2-minute mixing period and a 2-minute waiting period. The OCR over the 3-minute measurement period was calculated using the fixed delta technique for determining the slope. A bioenergetics profile composed of basal mitochondrial respiration, ATP turnover, H$^+$ leak, mitochondrial respiratory capacity, and nonmitochondrial respiration was determined by measuring the OCR in the basal state and following sequentially spaced injected oligomycin (10 µM), carbonyl cyanide p-trifluoromethoxyphenylhydrazone (FCCP) (1 µM), and rotenone (5 µM).

To measure oxygen consumption of mitochondria residing in the hypothalamus, hypothalamus of 6-month-old male mice was dissected using a mouse brain matrix (ASI Instruments), homogenized in IBc buffer (10 mM Tris-MOPS, 10 mM EGTA/Tris, 10 mM sucrose, 0.5% BSA) using a Dounce homogenizer (10 strokes), and centrifuged for 10 minutes at 600 *g*. Following centrifugation for 10 minutes at 7,000 *g*, the supernatants were discarded and the pellet was resuspended in 5 ml IBc buffer. After centrifugation (7,000 *g*, 10 minutes), the pellet was resuspended in 400 µl MAS buffer (70 mM sucrose, 220 mM mannitol, 10 mM KH$_2$PO$_4$, 5 mM MgCl$_2$, 2 mM HEPES, 1 mM EGTA, 0.2% BSA) and further processed for FACS analysis of mitochondrial mass or assessment of energy consumption. Here, 10 µg of mitochondria (in 4 to 5 replicates per genotype) were loaded on a 24-well XF24 V28 cell culture microplate and spun down for 10 minutes at 2,000 *g*. MAS buffer (450 µl) was added to each sample, and a bioenergetics profile consisting of basal mitochondrial respiration, ADP injection, ATP turnover, H$^+$ leak mitochondrial respiratory capacity, and nonmitochondrial respiration was determined by measuring the basal OCR and following sequentially spaced injected ADP (0.25 mM), oligomycin (2 µM), FCCP (4 µM), and antimycin A (4 µM). These experiments were independently repeated at least three times.

2-photon microscopy. Brain slices (1,000-µm-thick) of 6-month-old male mice containing the arcuate nucleus were cut using a mouse brain matrix and mounted in a 35-mm glass-bottom dish (P35G-1.0-20-C; MatTek) with a weight to stabilize for movement and drift. Brain slices were left to equilibrate for 2 hours before imaging at 37°C in artificial cerebrospinal fluid containing 25 mM glucose, 1.25 mM NaH$_2$PO$_4$, 25 mM NaHCO$_3$, 1 mM MgCl, 2 mM CaCl$_2$, 2.5 mM KCl, and 125 mM NaCl. Images were collected with a ×63, 1.2 NA Zeiss C-Apochromat objective on a Zeiss-LSM-710 microscope with the Cameleon infrared laser using 710 nm for excitation of riboflavins (NADH and FAD) as previously described (70). Riboflavin fluorescence was collected and descanned between 410 to 650 nm. Three brain regions in the arcuate nucleus were arbitrarily selected for Z-stack image collection. The Z-stacks were collected at a 30-µm distance from the brain slice surface. Images in the Z-stacks were collected every 1 µm, covering a distance of 30 µm into the slice, thus 30–60 µm. Areas were selected "blindly" at the surface of the brain slice, since the actual imaged regions deeper inside 30–60 µm were not visible in this Z-position. The TIF images of the Z-stacks obtained with Zeiss confocal software were imported into Metamorf Software (version 6.1; Universal Imaging Corp.). Image stacks covering the 45- to 60-µm distance were created. Maximal and sum projections were created and corrected for nonspecific background. Projection images were threshold adjusted and gray values were measured using Metamorf Software and exported into Excel. Gray value means of the three positions from each brain-slice region were imported into SigmaPlot 11.0 software.

Insulin sensitivity and leptin stimulation. Thirteen- to 14-week-old mice were fasted for 24 hours and injected with 5 U of insulin or saline (control) into the vena cava. The arcuate nucleus was isolated 10 minutes after injection, homogenized in 100 µl RIPA buffer using a mortar, and centrifuged for 15 minutes at 21,130 *g*. The supernatant was transferred into a new Eppendorf tube, and protein concentration was determined. Protein lysates (10 µg) were used for Western blot analysis.

Ten-week-old and 6-month-old male ob/ob mice were twice-daily injected with 2 mg/kg leptin or saline (control) into the peritoneum. Two hours after the second leptin treatment, arcuate nucleus was isolated and protein lysates used for Western blot analysis. Ten-week-old C57BL/6 mice were fasted for 18 hours and were twice-daily injected with 3 mg/kg leptin before and after fasting. Two hours after the second leptin treatment, arcuate nucleus was isolated and protein lysates used for Western blot analysis

Refeeding experiment. Ten-week-old C57BL/6 mice were fasted for 24 hours and refed ad libitum for 16 hours. Arcuate nucleus was isolated at indicated time points, and protein was extracted and processed for Western blot analysis.

Glucose and insulin tolerance test. A glucose tolerance test was performed in overnight-fasted, 12-week-old mice that were injected i.p. with 2 g dextrose per kilogram of body weight. Insulin tolerance tests were performed in 16-week-old randomly fed mice (1.25 U insulin per kilogram of body weight injected i.p. (Humulin R; Lilly).

Intrahypothalamic injection of lentiviral constructs. Ten-week-old male C57Bl/6 mice were placed in a stereotactic device under anesthesia, and a 33-gauge cannula (Plastics One, Inc.) was inserted into the hypothalamus (0.5 mm posterior ± 0.5 mm lateral and 5.7 mm ventral from the bregma) as previously described (71). shRNA lentiviral vector containing scrambled or shRNA directed against HSP60 was injected bilaterally into the ventral hypothalamus. Mice were single caged, and food intake was measured 48 hours after surgery for 5 days.

Transfection and luciferase assay. Cells (10^6) were transfected with a total of 10 µg of Stat3 Y705F Flag pRc/CMV (8709; Addgene) or Stat3 Flag pRc/CMV vector (8707; Addgene) (72) using SuperFect (QIAGEN) according to the manufacturer's guidelines. For the luciferase assay, 10^6 cells were transfected with a total of 10 µg pGL3 luciferase reporter vector as a control or human HSP60 promoter pGL3 luciferase reporter vector (73) in combination with pRL-0 *Renilla* luciferase vector (serving as a control for transfection efficiency). Transfected cells were plated on a 24-well plate. The following day, cells were starved for 10 hours, followed by 10 nM leptin, 10% FCS, or nonstimulation for 1 hour. Cells were harvested and

lysates analyzed using the Promega Dual Stop & Glo system according to the manufacturer's instructions.

Statistics. Data sets were analyzed for statistical significance using a two-tailed unpaired Student's *t* test. *P* values less than 0.05 were considered significant.

1. Szendroedi J, Phielix E, Roden M. The role of mitochondria in insulin resistance and type 2 diabetes mellitus. *Nat Rev Endocrinol.* 2012;8(2):92–103.
2. Evans JL, Maddux BA, Goldfine ID. The molecular basis for oxidative stress-induced insulin resistance. *Antioxid Redox Signal.* 2005;7(7–8):1040–1052.
3. Warner DS, Sheng H, Batinic-Haberle I. Oxidants, antioxidants and the ischemic brain. *J Exp Biol.* 2004;207(pt 18):3221–3231.
4. Halliwell B. Reactive oxygen species and the central nervous system. *J Neurochem.* 1992;59(5):1609–1623.
5. Chowdhury SK, et al. Mitochondrial respiratory chain dysfunction in dorsal root ganglia of streptozotocin-induced diabetic rats and its correction by insulin treatment. *Diabetes.* 2010;59(4):1082–1091.
6. Akude E, Zherebitskaya E, Chowdhury SK, Smith DR, Dobrowsky RT, Fernyhough P. Diminished superoxide generation is associated with respiratory chain dysfunction and changes in the mitochondrial proteome of sensory neurons from diabetic rats. *Diabetes.* 2011;60(1):288–297.
7. Santos MS, Santos DL, Palmeira CM, Seica R, Moreno AJ, Oliveira CR. Brain and liver mitochondria isolated from diabetic Goto-Kakizaki rats show different susceptibility to induced oxidative stress. *Diabetes Metab Res Rev.* 2001;17(3):223–230.
8. Thaler JP, et al. Obesity is associated with hypothalamic injury in rodents and humans. *J Clin Invest.* 2012;122(1):153–162.
9. Pipatpiboon N, Pratchayasakul W, Chattipakorn N, Chattipakorn SC. PPARgamma agonist improves neuronal insulin receptor function in hippocampus and brain mitochondria function in rats with insulin resistance induced by long term high-fat diets. *Endocrinology.* 2012;153(1):329–338.
10. Reading DS, Hallberg RL, Myers AM. Characterization of the yeast HSP60 gene coding for a mitochondrial assembly factor. *Nature.* 1989;337(6208):655–659.
11. Zeilstra-Ryalls J, Fayet O, Georgopoulos C. The universally conserved GroE (Hsp60) chaperonins. *Annu Rev Microbiol.* 1991;45:301–325.
12. Cheng MY, et al. Mitochondrial heat-shock protein hsp60 is essential for assembly of proteins imported into yeast mitochondria. *Nature.* 1989;337(6208):620–625.
13. Ostermann J, Horwich AL, Neupert W, Hartl FU. Protein folding in mitochondria requires complex formation with hsp60 and ATP hydrolysis. *Nature.* 1989;341(6238):125–130.
14. Cabiscol E, Belli G, Tamarit J, Echave P, Herrero E, Ros J. Mitochondrial Hsp60, resistance to oxidative stress, and the labile iron pool are closely connected in Saccharomyces cerevisiae. *J Biol Chem.* 2002;277(46):44531–44538.
15. Levy-Rimler G, Bell RE, Ben-Tal N, Azem A. Type I chaperonins: not all are created equal. *Growth Regul.* 2002;529(1):1–5.
16. Hemmingsen SM, et al. Homologous plant and bacterial proteins chaperone oligomeric protein assembly. *Nature.* 1988;333(6171):330–334.
17. Christensen JH, et al. Inactivation of the hereditary spastic paraplegia-associated Hspd1 gene encoding the Hsp60 chaperone results in early embryonic lethality in mice. *Cell Stress Chaperones.* 2010;15(6):851–863.
18. Hansen JJ, et al. Hereditary spastic paraplegia SPG13 is associated with a mutation in the gene encoding the mitochondrial chaperonin Hsp60. *Am J Hum Genet.* 2002;70(5):1328–1332.
19. Magen D, et al. Mitochondrial hsp60 chaperonopathy causes an autosomal-recessive neurodegenerative disorder linked to brain hypomyelination and leukodystrophy. *Am J Hum Genet.* 2008;83(1):30–42.
20. Bonior J, Jaworek J, Konturek SJ, Pawlik WW. Leptin is the modulator of HSP60 gene expression in AR42J cells. *J Physiol Pharmacol.* 2006;57(suppl 7):135–143.
21. Guo Z, Jiang H, Xu X, Duan W, Mattson MP. Leptin-mediated cell survival signaling in hippocampal neurons mediated by JAK STAT3 and mitochondrial stabilization. *J Biol Chem.* 2008;283(3):1754–1763.
22. Carvalheira JB, et al. Cross-talk between the insulin and leptin signaling systems in rat hypothalamus. *Obes Res.* 2005;13(1):48–57.
23. Koch C, et al. Leptin rapidly improves glucose homeostasis in obese mice by increasing hypothalamic insulin sensitivity. *J Neurosci.* 2010;30(48):16180–16187.
24. Schwartz MW, Porte D. Diabetes, obesity, and the brain. *Science.* 2005;307(5708):375–379.
25. McKeel DW, Jarett L. Preparation and characterization of a plasma membrane fraction from isolated fat cells. *J Cell Biol.* 1970;44(2):417–432.
26. Norenberg MD, Rao KV. The mitochondrial permeability transition in neurologic disease. *Neurochem Int.* 2007;50(7–8):983–997.
27. Hernandez-Fonseca JP, et al. Structural and ultrastructural analysis of cerebral cortex, cerebellum, and hypothalamus from diabetic rats. *Exp Diabetes Res.* 2009;2009:329632.
28. Buchner J, et al. GroE facilitates refolding of citrate synthase by suppressing aggregation. *Biochemistry.* 1991;30(6):1586–1591.
29. Myers MG, Cowley MA, Munzberg H. Mechanisms of leptin action and leptin resistance. *Annu Rev Physiol.* 2008;70:537–556.
30. Vaisse C, Halaas JL, Horvath CM, Darnell JE, Stoffel M, Friedman JM. Leptin activation of Stat3 in the hypothalamus of wild-type and ob/ob mice but not db/db mice. *Nat Genet.* 1996;14(1):95–97.
31. Kim SW, Kim JB, Kim JH, Lee JK. Interferon-gamma-induced expressions of heat shock protein 60 and heat shock protein 10 in C6 astroglioma cells: identification of the signal transducers and activators of transcription 3-binding site in bidirectional promoter. *Neuroreport.* 2007;18(4):385–389.
32. Bates SH, et al. STAT3 signalling is required for leptin regulation of energy balance but not reproduction. *Nature.* 2003;421(6925):856–859.
33. Fridlyand LE, Philipson LH. Reactive species and early manifestation of insulin resistance in type 2 diabetes. *Diabetes Obes Metab.* 2006;8(2):136–145.
34. Bjorbaek C, Elmquist JK, Frantz JD, Shoelson SE, Flier JS. Identification of SOCS-3 as a potential mediator of central leptin resistance. *Mol Cell.* 1998;1(4):619–625.
35. Emanuelli B, Peraldi P, Filloux C, Sawka-Verhelle D, Hilton D, Van Obberghen E. SOCS-3 is an insulin-induced negative regulator of insulin signaling. *J Biol Chem.* 2000;275(21):15985–15991.
36. Niswender KD, Morton GJ, Stearns WH, Rhodes CJ, Myers MG, Schwartz MW. Intracellular signalling. Key enzyme in leptin-induced anorexia. *Nature.* 2001;413(6858):794–795.
37. Bruning JC, et al. Role of brain insulin receptor in control of body weight and reproduction. *Science.* 2000;289(5487):2122–2125.
38. Konner AC, et al. Insulin action in AgRP-expressing neurons is required for suppression of hepatic glucose production. *Cell Metab.* 2007;5(6):438–449.
39. Inoue H, et al. Role of hepatic STAT3 in brain-insulin action on hepatic glucose production. *Cell Metab.* 2006;3(4):267–275.
40. Tung YC, Ma M, Piper S, Coll A, O'Rahilly S, Yeo GS. Novel leptin-regulated genes revealed by transcriptional profiling of the hypothalamic paraventricular nucleus. *J Neurosci.* 2008;28(47):12419–12426.
41. Edwards JL, et al. Diabetes regulates mitochondrial biogenesis and fission in mouse neurons. *Diabetologia.* 2010;53(1):160–169.
42. Jheng HF, et al. Mitochondrial fission contributes to mitochondrial dysfunction and insulin resistance in skeletal muscle. *Mol Cell Biol.* 2012;32(2):309–319.
43. Franklin JL, Keeton AB, Bortoff KD, Messina JL. Insulin dependant gene expression of heat shock protein 60 in H4IIE hepatoma cells. *Int J Clin Exp Med.* 2008;1(1):89–97.
44. Lin J, et al. Defects in adaptive energy metabolism with CNS-linked hyperactivity in PGC-1alpha null mice. *Cell.* 2004;119(1):121–135.
45. Zechner C, et al. Total skeletal muscle PGC-1 deficiency uncouples mitochondrial derangements from fiber type determination and insulin sensitivity. *Cell Metab.* 2010;12(6):633–642.
46. Muniyappa R, Lee S, Chen H, Quon MJ. Current approaches for assessing insulin sensitivity and resistance in vivo: advantages, limitations, and appropriate usage. *Am J Physiol Endocrinol Metab.* 2008;294(1):E15–E26.
47. Larsson N, et al. Mitochondrial transcription factor A is necessary for mtDNA maintenance and embryogenesis in mice. *Nat Genet.* 1998;18(3):231–236.
48. Chan JY, et al. Targeted disruption of the ubiquitous CNC-bZIP transcription factor, Nrf-1, results in anemia and embryonic lethality in mice. *EMBO J.* 1998;17(6):1779–1787.
49. Floyd RA. Antioxidants, oxidative stress, and degenerative neurological disorders. *Proc Soc Exp*

Biol Med. 1999;222(3):236–245.

50. Ernst MB, et al. Enhanced Stat3 activation in POMC neurons provokes negative feedback inhibition of leptin and insulin signaling in obesity. *J Neurosci.* 2009;29(37):11582–11593.

51. Olofsson LE, Unger EK, Cheung CC, Xu AW. Modulation of AgRP-neuronal function by SOCS3 as an initiating event in diet-induced hypothalamic leptin resistance. *Proc Natl Acad Sci U S A.* 2013;110(8):E697–E706.

52. Haber CA, et al. N-acetylcysteine and taurine prevent hyperglycemia-induced insulin resistance in vivo: possible role of oxidative stress. *Am J Physiol Endocrinol Metab.* 2003;285(4):E744–E753.

53. Lee HY, et al. Targeted expression of catalase to mitochondria prevents age-associated reductions in mitochondrial function and insulin resistance. *Cell Metab.* 2010;12(6):668–674.

54. Lortz S, Tiedge M. Sequential inactivation of reactive oxygen species by combined overexpression of SOD isoforms and catalase in insulin-producing cells. *Free Radic Biol Med.* 2003;34(6):683–688.

55. Krieger-Brauer HI, Kather H. Human fat cells possess a plasma membrane-bound H_2O_2-generating system that is activated by insulin via a mechanism bypassing the receptor kinase. *J Clin Invest.* 1992;89(3):1006–1013.

56. Ristow M, et al. Antioxidants prevent health-promoting effects of physical exercise in humans. *Proc Natl Acad Sci U S A.* 2009;106(21):8665–8670.

57. Mahadev K, Zilbering A, Zhu L, Goldstein BJ. Insulin-stimulated hydrogen peroxide reversibly inhibits protein-tyrosine phosphatase 1b in vivo and enhances the early insulin action cascade. *J Biol Chem.* 2001;276(24):21938–21942.

58. Accili D, et al. Early neonatal death in mice homozygous for a null allele of the insulin receptor gene. *Nat Genet.* 1996;12(1):106–109.

59. Bruning JC, Winnay J, Bonner-Weir S, Taylor SI, Accili D, Kahn CR. Development of a novel polygenic model of NIDDM in mice heterozygous for IR and IRS-1 null alleles. *Cell.* 1997;88(4):561–572.

60. Ozcan U, et al. Endoplasmic reticulum stress links obesity, insulin action, and type 2 diabetes. *Science.* 2004;306(5695):457–461.

61. Bruce CR, Carey AL, Hawley JA, Febbraio MA. Intramuscular heat shock protein 72 and heme oxygenase-1 mRNA are reduced in patients with type 2 diabetes: evidence that insulin resistance is associated with a disturbed antioxidant defense mechanism. *Diabetes.* 2003;52(9):2338–2345.

62. Chung J, et al. HSP72 protects against obesity-induced insulin resistance. *Proc Natl Acad Sci U S A.* 2008;105(5):1739–1744.

63. Gupte AA, Bomhoff GL, Swerdlow RH, Geiger PC. Heat treatment improves glucose tolerance and prevents skeletal muscle insulin resistance in rats fed a high-fat diet. *Diabetes.* 2009;58(3):567–578.

64. Rizzetto L, Zanni E, Uccelletti D, Ferrero I, Goffrini P. Extension of chronological lifespan by hexokinase mutation in Kluyveromyces lactis involves increased level of the mitochondrial chaperonin Hsp60. *J Aging Res.* 2012;2012:946586.

65. Salway KD, Gallagher EJ, Page MM, Stuart JA. Higher levels of heat shock proteins in longer-lived mammals and birds. *Mech Ageing Dev.* 2011;132(6–7):287–297.

66. Xanthoudakis S, et al. Hsp60 accelerates the maturation of pro-caspase-3 by upstream activator proteases during apoptosis. *EMBO J.* 1999;18(8):2049–2056.

67. Gupta S, Knowlton AA. HSP60, Bax, apoptosis and the heart. *J Cell Mol Med.* 2005;9(1):51–58.

68. Magnoni R, et al. Late onset motoneuron disorder caused by mitochondrial Hsp60 chaperone deficiency in mice. *Neurobiol Dis.* 2013;54:12–23.

69. Sonnen JA, et al. Different patterns of cerebral injury in dementia with or without diabetes. *Arch Neurol.* 2009;66(3):315–322.

70. Huang S, Heikal AA, Webb WW. Two-photon fluorescence spectroscopy and microscopy of NAD(P)H and flavoprotein. *Biophys J.* 2002;82(5):2811–2825.

71. Suzuki R, et al. Diabetes and insulin in regulation of brain cholesterol metabolism. *Cell Metab.* 2010;12(6):567–579.

72. Wen Z, Darnell JE. Mapping of Stat3 serine phosphorylation to a single residue (727) and evidence that serine phosphorylation has no influence on DNA binding of Stat1 and Stat3. *Nucleic Acids Res.* 1997;25(11):2062–2067.

73. Hansen JJ, et al. Genomic structure of the human mitochondrial chaperonin genes: HSP60 and HSP10 are localised head to head on chromosome 2 separated by a bidirectional promoter. *Hum Genet.* 2003;112(1):71–77.